Proceedings of the 17th World Congress
The International Federation of Automatic Control
Seoul, Korea, July 6-11, 2008

Hysteresis Inverse Iterative Learning Control of Piezoactuators in AFM

S. C. Ashley, U. Arıdoğan, R. Riddle, K. K. Leang ⋆

Department of Mechanical Engineering
Virginia Commonwealth University
Richmond, VA 23284, USA

Abstract: We consider the application of iterative learning control (ILC) in which the input update law exploits an inverse model of the hysteresis behavior for piezoactuators. Compared to ILC for hysteresis that updates the control input using the measured tracking error scaled by a constant (fixed) learning gain, the proposed ILC algorithm converges more rapidly. The approach is analyzed and experimental results are presented to demonstrate the method's ability for precision output tracking.

1. INTRODUCTION

The atomic force microscope (AFM), a type of scanning probe microscope (SPM), can observe, manipulate, and fabricate intricate features well below the nanometer range. The AFM is an important tool in nanotechnology (Wiesendanger [1994]), where it is used to position atoms, image the structure of biological specimens such as DNA, fabricate novel nanoscale structures like quantum dots, and measure the elastic properties of organic and inorganic materials.

One critical component of AFM, and SPM's in general, is the piezoactuator. The piezoactuator is used to position the AFM probe tip relative to a sample's surface (Binnig [1992]). Although the piezoactuator is capable of high resolution positioning, it exhibits hysteresis and dynamic effects (Croft et al. [2001]). These effects cause significant positioning errors (Barrett and Quate [1991]), and the errors then lead to distortion of AFM images, as well as poor tolerances in the shape, size, and distribution of features made with AFM-based techniques (Snow et al. [1997]). Therefore, precise positioning of the piezoactuator in SPM's is needed, for example, to create well-defined patterns of nanofeatures such as quantum dots (Taylor et al. [2005]).

Feedforward and feedback controllers can minimize hysteresis in piezoactuators. For example, the Preisach model has been exploited for feedforward compensation of the hysteresis effect (Ge and Jouaneh [1995], Croft et al. [2001], Song et al. [2005]). Likewise, feedback control can reduce the hysteresis-caused positioning error in piezo-based systems (Barrett and Quate [1991], Salapaka et al. [2002]). One major drawback of model-based feedforward control is lack of robustness. As the system ages, it changes and can be affected by temperature variations; therefore, modeling errors can degrade the performance of model-based feedforward controllers. In feedback control, the sensor noise, which enters through the feedback link, can limit the performance (Gopal [2002]). Additionally, high feedback gains may be difficult to achieve when the system's gain margin is low (Leang and Devasia [2007]). Integrated feedback and feedforward controllers can compensate for the lack of robustness, as well as the use of approximate models for feedforward (Smith et al. [2000]). An alternative to feedforward and feedback control of hysteresis in piezoactuators is charge control (Fleming and Moheimani [2005]).

When AFM is used for imaging or nanofabrication, the piezoactuator moves the probe tip over the sample surface in a repetitive fashion. This repetitive process was exploited to compensate for hysteresis. Iterative learning control (ILC) is a method by which an input is found through repetition to track a desired trajectory (Arimoto et al. [1984], Moore et al. [1992]). ILC has been applied to account for hysteresis effect in several hysteretic systems (Hu et al. [2004], Iyer et al. [2005], Leang and Devasia [2006]). One simple ILC algorithm proposed was based on *proportional* feedback of the error signal at the current iteration step (Iyer et al. [2005], Leang and Devasia [2006]). In this case the iteration gain that scales the tracking error at each iteration step was chosen as a sufficiently small constant. Although the convergence was studied, the constant gain is conservative. Therefore, the convergence rate of such ILC design is slow. Practically speaking, the drawback of slow convergence is having to wait for many iterations before the tracking error diminishes to an acceptable value.

Faster convergence of ILC can be achieved by exploiting more information about the system. This concept was analyzed and applied to an electrostrictive device where the hysteresis behavior was assumed to be quadratic and memoryless (Hu et al. [2004]). But unfortunately, the hysteresis effect in systems such as piezoactuators (Ge and Jouaneh [1995]) and shape memory alloys (Gorbet et al. [1998]) depend on past input history, hence their input-output behavior are multi-valued and history dependent (Brokate and Sprekels [1996], Mayergoyz [1991]).

The contribution of this work is developing an ILC algorithm which offers improved performance compared to the standard *proportional* scheme. The proposed algorithm

⋆ Corresponding author; Voice/Fax: +1.804.827.7037/7030; Email: kkleang@vcu.edu.

incorporates an inverse hysteresis model. In contrast to the model-based approach proposed in (Hu et al. [2004]), the proposed method exploits the Preisach hysteresis model that captures the effect of past input history. The ILC scheme can be integrated with existing feedback controllers in AFM's to provide robustness. We present the details of the algorithm and then apply it to AFM fabrication. Experimental results are presented to demonstrate enhanced performance. Section 2 reviews the ILC approach for hysteresis. A modified algorithm is presented in Section 3, followed by experimental results in Section 4. Finally, concluding remarks are found in Section 5.

2. HYSTERESIS MODEL AND ILC

We let $I \triangleq [t_0, t_f]$ denote the finite time interval from time t_0 to t_f. The set of all continuous nondecreasing (respectively nonincreasing) functions on the interval I is represented by $C^0_{m+}(I)$ (respectively $C^0_{m-}(I)$).

2.1 The Preisach Hysteresis Model and Useful Properties

The focus here is hysteresis behavior, which is assumed to be rate-independent, therefore we neglect dynamic effects. ILC for combined hysteresis and dynamics is addressed in (Wu and Zou [2007]). The Preisach hysteresis model has been studied extensively to characterize the rate-independent hysteresis in piezoelectric materials, *e.g.*, see (Ge and Jouaneh [1995]). In the Preisach model, output $v(t)$ of a hysteretic system is

$$v(t) = \mathcal{H}[u](t) \triangleq \iint_{\alpha \geq \beta} \mu(\alpha, \beta) \mathcal{R}_{\alpha,\beta}[u](t) d\alpha d\beta. \qquad (1)$$

In (1), $\mu(\alpha, \beta)$ is the Preisach weighting function and the point (α, β) belongs in the restricted Preisach plane $\mathbf{P}$, defined as

$$\mathbf{P} \triangleq \{(\alpha, \beta) | \alpha \geq \beta; \underline{u} \leq \alpha; \beta \leq \bar{u}\}. \qquad (2)$$

In practice, Eq. (2) implies that only relays enclosed in the right-triangle region are affected by the input u.

Assumption 1. (Nonnegative μ) The Preisach weighting function is piecewise continuous, nonnegative, and bounded over the Preisach plane $\mathbf{P}$, *i.e.*, $0 \leq \mu(\alpha, \beta) \leq \infty$, $\forall (\alpha, \beta) \in \mathbf{P}$.

Remark 1. Assumption 1 ensures that if the input $u(t)$ is increasing (resp. decreasing) in time, then its associated output $v(t)$ is also increasing (resp. decreasing) in time (Visintin [1993]). Therefore, the rate of change in the output with respect to the input is positive.

Definition 1. (Branch). Let L_0 be an initial memory curve and $u \in C^0_{m+}(I)$ (respectively, $u \in C^-_{m-}(I)$), then we say the pair $(u, \mathcal{H}[u])$ belongs to the branch $\mathcal{B}_\uparrow[\cdot, L_0]$ (respectively $\mathcal{B}_\downarrow[\cdot, L_0]$). A branch is monotonic in the input u.

Property 1. (Bounds on the output difference). Let the Preisach model Assumption 1 hold and L_0 be an initial memory curve. Given $u_1, u_2 \in C^0_{m+}(I)$ (respectively, $u_1, u_2 \in C^0_{m-}(I)$) such that $(u_1, \mathcal{H}[u_1])$, $(u_2, \mathcal{H}[u_2]) \in \mathcal{B}_\uparrow[\cdot, L_0]$ (respectively, $(u_1, \mathcal{H}[u_1]), (u_2, \mathcal{H}[u_2]) \in \mathcal{B}_\downarrow[\cdot, L_0]$) and if $u_1(t_1) \leq u_2(t_2)$ for any $t_1, t_2 \in I$, then

$$\eta_1 \big(u_2(t_2) - u_1(t_1)\big)^n \leq \mathcal{H}[u_2](t_2) - \mathcal{H}[u_1](t_1) \leq \eta_2 \big(u_2(t_2) - u_1(t_1)\big), \qquad (3)$$

where n is a positive integer. The upper and lower bounds in (3) can be found as described in (Leang and Devasia [2006]).

2.2 Iterative Learning Control for Hysteresis Effect

Given a desired trajectory $v_d(t)$ for $t \in I \triangleq [t_0, t_f]$, the objective of ILC is to iteratively find an input $u_d(t)$ such that $v_d(t) = \mathcal{H}[u_d](t)$. Hysteresis compensation is achieved using an iterative learning control algorithm (ILCA) of the following form (Iyer et al. [2005], Leang and Devasia [2006]):

$$u_{k+1}(t) = u_k(t) + \rho \big(v_d(t) - v_k(t)\big), \qquad \forall t \in I, \qquad (4)$$

where k is the trial (iteration) number, $u_{k+1}(t)$ and $u_k(t)$ are the next and current input at time t, $v_k(t)$ is the current output value, and ρ is the iteration gain (a constant). To ensure that ILCA (4) converges to the desired input $u_d(\cdot)$ as $k \to \infty$, we require (Leang and Devasia [2006]):

- $\mathcal{C}1$) The initial condition at t_0 must be the same for every iteration step k. To achieve this, an appropriate input is applied to *reset* the Preisach memory curve $L(t)$ such that at the initial time t_0, the initial memory curve $L_0 \triangleq L(t_0)$ is the same for every step k;
- $\mathcal{C}2$) The desired trajectory is monotonic; and
- $\mathcal{C}3$) The iteration gain ρ must be sufficiently small.

$$0 < \rho \leq \begin{cases} \min\left\{\dfrac{1}{\eta_2}, \dfrac{2}{\eta_1}\right\}; & \text{if } n = 1, \\ \min\left\{\dfrac{1}{\eta_2}, \dfrac{2}{\eta_1(\overline{u} - \underline{u})}\right\}; & \text{if } n = 2. \end{cases} \qquad (5)$$

The performance of ILCA (4) is governed by the bounds on the output difference (3). The bounds determine the iteration gain ρ.

3. HYSTERESIS INVERSE ILC

The ILC algorithm (4) leads to slow convergence because the iteration gain ρ based on the bounds on the output difference (3) is conservative (Tchoupo and Leang [2007]). The inverse hysteresis model was utilized to improve performance.

Assumption 2. (Invertibility) On a branch (*e.g.*, $\mathcal{B}_\uparrow[\cdot, L_0]$), the Preisach hysteresis model is invertible; that is, for a given $v(t)$ for $t \in [t_0, t]$ and some initial inverse memory curve L_0^{-1}, $u(\cdot) = \mathcal{H}^{-1}[v](\cdot)$. Furthermore, we assume the difference in the output of the inverse model for any $t_1, t_2 \in I$ on a branch is

$$\xi_1 \big(v_2(t_2) - v_1(t_1)\big)^m \leq \mathcal{H}^{-1}[v_2](t_2) - \mathcal{H}^{-1}[v_1](t_1) \leq \xi_2 \big(v_2(t_2) - v_1(t_1)\big), \qquad (6)$$

where m is a positive integer.

By Assumption 2, for a given output $v(t) = \mathcal{H}[u](t)$, we have $u(t) = \mathcal{H}^{-1}[v](t)$. Then an input-update law that incorporates the inverse model $\mathcal{H}^{-1}[\cdot]$ can be written as

$$u_{k+1}(t) = u_k(t) + \mathcal{H}^{-1}[v_d](t) - \mathcal{H}^{-1}[v_k](t),$$

for $t \in I$.

With a perfect model $\mathcal{H}[\cdot]$, we can achieve convergence in one step. In practice, however, the model will have an uncertainty. Therefore, we introduce the constant α,

$$u_{k+1}(t) = u_k(t) + \alpha\Big(\mathcal{H}^{-1}[v_d](t) - \mathcal{H}^{-1}[v_k](t)\Big). \quad (7)$$

The constant α must be chosen to ensure that the inverse-based ILCA (7) converges. In particular, we seek the bounds on α such that the pair $(v_k(t), u_k(t))$, for $t \in I$, belongs on a single hysteresis branch for every k. In other words, the ILCA must preserve the monotonicity of the input from one iteration to the next (Leang and Devasia [2006]).

Assumption 3. Given $v_k(t) \leq v_d(t)$ and let L_0^{-1} be the memory curve associated with the inverse hysteresis model $\mathcal{H}^{-1}[\cdot]$. We assume that the error in computing the step size from $\mathcal{H}^{-1}$ is

$$\Delta\hat{u}_k(t) = \Delta u_k(t) + \epsilon_u\big(\Delta v_k(t)\big), \quad (8)$$

where $\Delta v_k(t) = v_d(t) - v_k(t)$ is the output error and $\Delta u_k(t)$ denotes the actual step size (error in the input given a perfect model). Additionally, we assume that the function $\epsilon_u(\cdot)$ is monotonic in the output difference Δv_k and

$$\epsilon_u\big(\Delta v_k(t)\big) = 0 \quad (9)$$

when $\Delta v_k(t) = 0$ for any $t \in I$; also, there exists a constant $0 < M < \infty$ such that

$$\epsilon_u\big(\Delta v_k(t)\big) \leq M\Delta v_k(t). \quad (10)$$

Proposition 1. Let Assumptions 1, 2, and 3 be satisfied. If $0 < \alpha \leq \xi_1/(\xi_2 + M)$, then the ILCA (7) generates a sequence of inputs such that $u_k(t) \leq u_d(t)$ for all $t \in I$, and $k \geq 1$. Hence, the step size generated by the ILCA (7) does not *overshoot* the desired input u_d for all k.

Proof: By ILCA (7), the step size for the k^{th} iteration is

$$\alpha\Delta\hat{u}_k = \alpha\big[\Delta u_k(t) + \epsilon_u\big(\Delta v_k(t)\big)\big]. \quad (11)$$

The objective is to determine an α such that

$$\alpha\big[\Delta u_k(t) + \epsilon_u\big(\Delta v_k(t)\big)\big] \leq \Delta u_k(t), \quad (12)$$

which implies

$$\alpha \leq \frac{\Delta u_k(t)}{\Delta u_k(t) + \epsilon_u\big(\Delta v_k(t)\big)}. \quad (13)$$

With Assumption 3 and the bounds on the input difference (6), we find that

$$\begin{aligned}\frac{\xi_1\Delta v_k(t)}{\xi_2\Delta v_k(t) + M\Delta v_k(t)} &\leq \frac{\Delta u_k(t)}{\Delta u_k(t) + M\Delta v_k(t)} \\ &\leq \frac{\Delta u_k(t)}{\Delta u_k(t) + \epsilon_u\big(\Delta v_k(t)\big)}. \end{aligned} \quad (14)$$

Hence, $0 < \alpha \leq \xi_1/(\xi_2 + M)$. □

The results of Proposition 1 ensures that the sequence of inputs generated by the ILCA (7) remains monotonic in time, and of the same sign in monotonicity as the desired trajectory v_d. As a result, $(v_k(t), u_k(t))$, for $t \in I$, belongs on a single hysteresis branch.

Proposition 2. Let Assumptions 1, 2, and 3 be satisfied. Let $v_d \in C_{m+}(I)$ [respectively $u_0 \in C_{m-}(I)$] and pick $u_0 \in C_{m+}(I)$ [respectively $u_0 \in C_{m-}(I)$]. If $0 < \alpha \leq \min\{\xi_1/(\xi_2 + M), 2\}$, then the ILCA (7) converges, *i.e.*, $u_k \to u_d$ as $k \to \infty$.

Proof: From ILCA (7), we have the following:

$$\begin{aligned} u_{k+1}(t) &= u_k(t) + \alpha\Delta\hat{u}_k(t), \\ &= u_k(t) + \alpha\Delta u_k(t) + \alpha\epsilon_u\big(\Delta v_k(t)\big). \end{aligned} \quad (15)$$

Subtracting the above expression from $u_d(t)$ and applying Assumption 3 and the output bound (3), we can bound the input error as follows:

$$\begin{aligned} \Delta u_{k+1}(t) &\leq \Delta u_k(t) - \alpha\Delta u_k(t), \\ \Delta u_{k+1}(t) &\leq \big(1 - \alpha\big)\Delta u_k(t). \end{aligned} \quad (16)$$

Taking the norm of both sides, we find for convergence that $0 < \alpha < 2$. Combining the results of Proposition 1, the restriction on α is $0 < \alpha \leq \min\{\xi_1/(\xi_2 + M), 2\}$. □

4. APPLICATION IN AFM FABRICATION

4.1 The Experimental System

The experimental AFM system is the Molecular Imaging (MI, now part of Agilent Technologies) PicoPlus model. In this AFM, the cantilever (with tip) is attached to the piezoactuator. The piezoactuator moves the cantilever and prove tip relative to a fixed sample (see Fig. 1).

The system was customized to permit the application of control signals in the three coordinate axes (x, y, and z) to control the piezoactuator. The output of the inductive sensors, which are used to measure the displacement of the piezo, were accessible through a custom signal access module. The gain of the inductive sensors are 3.59 μm/V in the x-axis and 4.04 μm/V in the y-axis. The MI software was used for imaging and to maintain constant deflection of the cantilever by controlling the z-axis during fabrication. An external computer and data acquisition system running custom C code was used to apply control signals and read the position sensor voltages.

We focus our attention in this study on hysteresis effect; therefore, the AFM was operated at low frequencies to avoid exciting the high-order dynamics (Croft et al. [2001]). The measured frequency response revealed dominant resonances at 417 Hz and 400 Hz for the x and y axis, respectively. Based on the frequency response, the fabrication process was chosen less than 1 Hz.

4.2 The Fabrication Process

The AFM can be used to fabricate features for creating novel nano-scale electronics and structures (Wendel et al. [1994]) as well as sensors (Davis et al. [2000]). The fabrication techniques include voltage-induced oxidation (Campbell and Snow [1996]), dip-pen lithography (Piner et al. [1999]), or physically indenting and scratching the surface (Kunze [2002]). Additionally, AFM can be used to manipulate particles (Decossas et al. [2003]). We considered the process of scratching features on a soft sample by physically embedding and "dragging" the AFM tip over the sample's surface. This approach is one of the simplest fabrication techniques, and the resulting features can be used to define a mask for lithography to create quantum devices (Wendel et al. [1994]). We note that precise tracking of the piezoactuator's trajectory is needed to create well-defined patterns of structures (Sohn and Willett [1995], Ortner et al. [2003]).

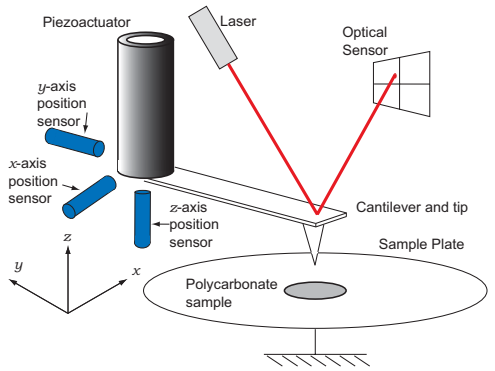

(a)

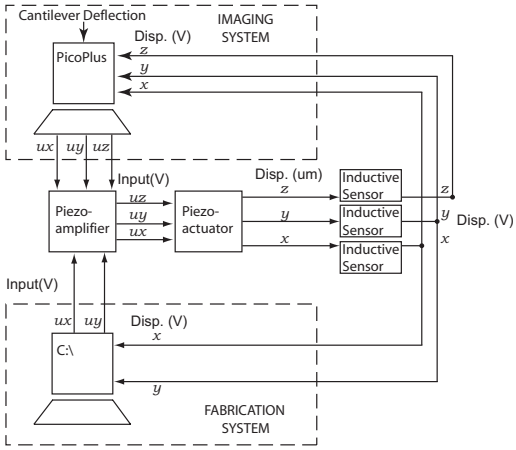

(b)

Fig. 1. The experimental AFM system: (a) A schematic of the main components; and (b) A block diagram of the system. A feedback controller (PicoPlus software) establishes constant deflection of the cantilever. The external computer running custom C code is used for implementing the ILC algorithm and it was also used to measure the sensor voltages in the x and y axes.

A circular feature in the x/y plane shown in Figs. 2 (a) and (b) was fabricated with the AFM. A relatively soft, polycarbonate surface was chosen as the medium for scratching. The polycarbonate sample has an elastic modulus of 2400 MPa. The fabrication process begins by first lowering the AFM tip (with spring constant 40 N/m) onto the sample surface, and once in contact with the sample, a relatively low force set point (approx. 0.5 μN) was used to image the sample. The imaging was performed under closed-loop PI control ($k_i = 1.2$, $k_p = 1.0$) using the MI software. Closed-loop imaging was done to obtain an accurate image of the surface, especially before and after application of ILC for comparison. After imaging, the piezoactuator was brought to the home position ($x = y = 0$) and the force set point was increased to approximately 7.5 μN for scratching. (We note that the value agrees with the work of other researchers, *e.g.*, see (Yan et al. [2007]). With the tip fully engaged, control voltages were then applied to the x and y axes of the piezoactuator from an external computer running custom C code. Once fabrication was complete, the force set point was reduced to 0.5 μN for imaging (in closed-loop) the sample.

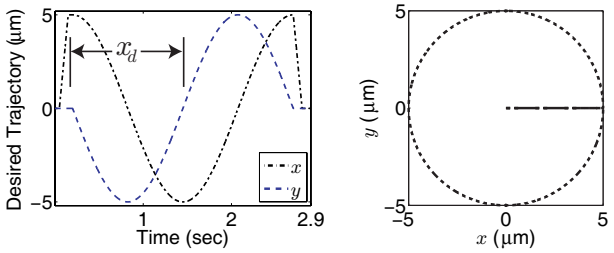

(a) (b)

Fig. 2. The desired trajectory in (a) the x and y axes and (b) a top view of the desired circular fabrication trajectory.

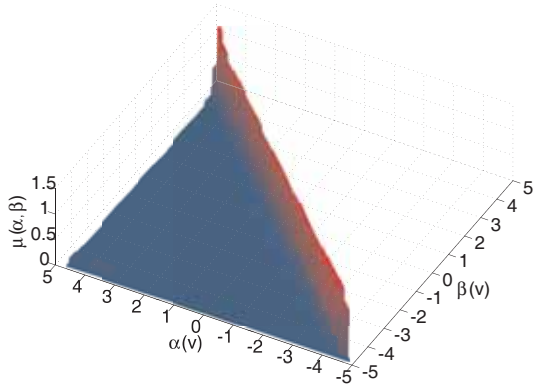

Fig. 3. Preisach weighting function for the piezoactuator in the x axis.

4.3 Application of ILC

In this section, we apply the ILC approach, comparing both the fixed learning gain method to the proposed inverse-based algorithm.

ILC can be used before engaging, then applied and even combined with feedback for added robustness to model uncertainty.

To determine an appropriate iteration gain for convergence, the hysteresis behavior was modeled using the Preisach approach. The model was obtained from input-output data using a least-squares method, and the approach is described in (Galinaitis and Rogers [1998]). Figure 3 shows the obtained Preisach weighting function $u(\cdot, \cdot)$ for the x axis. The y-axis model was similar. The maximum absolute and root-mean-square error between the model output and the measured output were 1.11% and 0.019%, respectively. Based on the model, an estimate of the iteration gain ρ for the fixed gain ILC was $0 < \rho \leq 0.062$. In the experiments, we chose the value $\rho = 0.05$ which falls within the acceptable range.

An inverse hysteresis model was also identified using the method described in (Croft et al. [2001]) for the inverse-based ILC. The inverse model was used to compute the gain α for the ILC feedforward input Eq. (7). A more simplified inverse model can be considered, for example, polynomial-based models can be used provided that the model captures the effect of input history.

Without ILC compensation, the effect of hysteresis in the piezoactuator causes significant tracking error and distortion during fabrication. Figure 4, plots (a) and

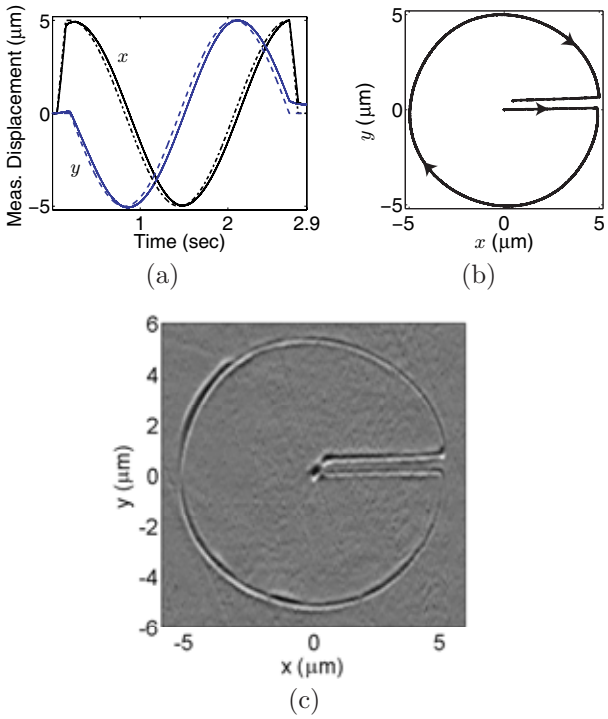

Fig. 4. The measured performance without ILC compensation: (a) The x and y trajectories versus time, (b) a top view of fabrication trajectory, and (c) an AFM image of the fabricated feature.

(b), and AFM image (c) show the effects of hysteresis, where the maximum tracking error in the x and y axes are, 13.48% and 14.5%, respectively. The polycarbonate substrate used was not flat and defects are evident.

To illustrate the ILC approach, we apply the method to the x-axis — the y-axis results are similar and omitted for brevity. The desired trajectory x_d of interest is shown in Fig. 2(a), and the time interval is $I = [0.2, 1.45]$ s. The desired trajectory is monotonic over the chosen time interval. For general trajectories, the ILCA is applied by partitioning the trajectory into multiple monotonic sections and moving from one section to the next. The details of this algorithm is described in (Leang and Devasia [2006]). In all the experiments, the system was reinitialized at the start of the desired trajectory, *i.e.*, $t_0 = 0.2$ s.

First, the constant iteration gain ILC, Eq. (4), was applied and after 120 iterations, the magnitude of the maximum tracking error is 0.5% (with respect to 10 μm range). The initial input u_0 was chosen as the desired trajectory scaled by a constant value. The tracking results at different iteration steps are shown in Fig. 5(a), along with the maximum error versus iteration step k shown in Fig. 5(b).

The inverse-based ILCA (7) was applied using the same desired trajectory x_d. The value of α was 0.05, 0.1, and 0.5. By incorporating the inverse, the proposed ILCA converges more rapidly. The tracking results at different iteration steps are shown in Fig. 5(a), along with the maximum error versus iteration step k shown in Fig. 5(b). The error versus k plot compares the results for the constant iteration gain to the inverse-based ILCA. With an $\alpha = 0.5$, after 11 iterations the maximum error of the inverse-based ILCA converges to 0.5%(see Fig. 6).

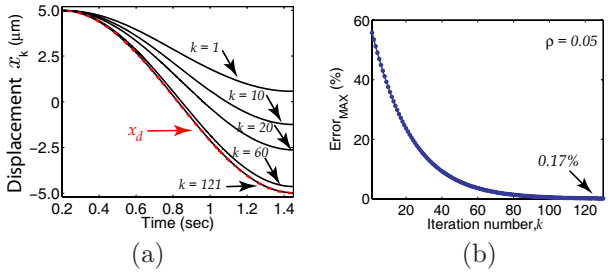

Fig. 5. Experimental results of ILC with constant iteration gain ($\rho = 0.05$): (a) The output for several trials; (b) The magnitude of maximum tracking error versus iteration number, k.

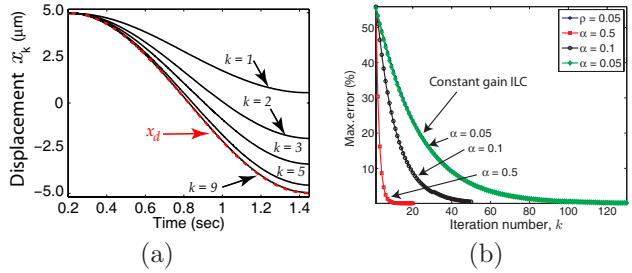

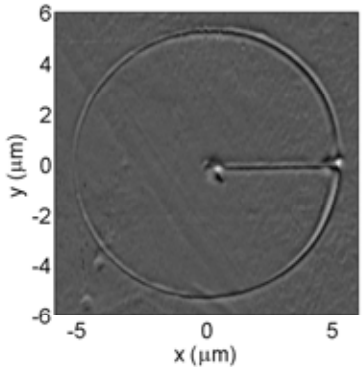

Fig. 6. Experimental results of inverse-hysteresis ILC: (a) The output for several trials ($\alpha = 0.5$); (b) The magnitude of maximum tracking error vs. iteration number, k, for the constant-gain ILC ($\rho = 0.05$) and inverse-hysteresis ILC ($\alpha = 0.5$, 0.1, 0.05). (c) AFM image of fabricated feature.

The improvement in the rate of convergence is ten-fold compared to the constant iteration gain approach. Figure 6(c) shows the fabrication results using the inverse-based ILCA, and the desired circular feature is achieved.

5. CONCLUSIONS

In this paper, we used the ILC method to compensate for hysteresis effect in piezoactuators. The ILC algorithm incorporated an approximate inverse hysteresis model. By using the model, a better estimate of the required step size for convergence was achieved. Compared to standard ILC where the update law is proportional to the tracking error, the model-based ILC yields improved rate of convergence. The ILC method was applied to fabricate a micro-sized feature using an experimental AFM and results were presented to demonstrate the effectiveness of the approach.

ACKNOWLEDGEMENTS

The authors thank Mike Freed for his help in the modeling process. This project was supported, in part, by the National Science Foundation DUE Grant #0633098.

REFERENCES

S. Arimoto, S. Kawamura, and F. Miyazaki. Bettering operation of dynamic systems by learning: a new control theory for servomechanism or mechatronics systems. In *Proc. American Control Conference*, pages 1064–1069, 1984.

R. C. Barrett and C. F. Quate. Optical scan-correction system applied to atomic force microscopy. *Rev. Sci. Instr.*, 62(6):1393–1399, 1991.

G. Binnig. Force microscopy. *Ultramicroscopy*, 42-44:7–15, 1992.

M. Brokate and J. Sprekels. *Hysteresis and phase transitions*. Springer, New York, 1996.

P. M. Campbell and E. S. Snow. Proximal probe-based fabrication of nanostructures. *Semicond. Sci. Technol.*, 11:1558–1562, 1996.

D. Croft, G. Shed, and S. Devasia. Creep, hysteresis, and vibration compensation for piezoactuators: atomic force microscopy application. *ASME J. Dyn. Syst., Meas., and Control*, 123:35–43, 2001.

Z. J. Davis, G. Abadal, O. Kuhn, O. Hansen, and A. Boisen. Fabrication and characterization of nanoresonating devices for mass detection. *J. Vac. Sci. Technol. B*, 18(2):612–616, 2000.

S. Decossas, F. Mazen, T. Baron, and G. Bremond A. Souifi. Atomic force microscopy nanomanipulation of silicon nanocrystals for nanodevice fabrication. *Nanotechnology*, 14:1272–1278, 2003.

A. J. Fleming and S. O. R. Moheimani. A grouned-load charge amplifier for reducing hysteresis in piezoelectric tube scanners. *Review of Scientific Instruments*, 76: 073707–1, 2005.

W. S. Galinaitis and R. C. Rogers. Control of a hysteretic actuator using inverse hysteresis compensation. In *SPIE Conf. on Mathematics and Control in Smart Structures*, volume 3323, pages 267–277, 1998.

P. Ge and M. Jouaneh. Modeling hysteresis in piezoceramic actuators. *Precision Engineering*, 17(3):211–221, 1995.

M. Gopal. *Control systems: principles and design*. McGraw Hill, New York, 2002.

R. B. Gorbet, D. W. L Wang, and K. A. Morris. Preisach model identification of a two-wire sma actuator. In *Proc. IEEE Int. Conf. on Robotics and Automation*, pages 2161–2167, Leuven, Belgium, 1998.

M. Hu, H. Du, S.-F. Ling, Z. Zhou, and Y. Li. Motion control of an electrostrictive actuator. *Mechatronics*, 14 (2):153–161, 2004.

R. V. Iyer, X. Tan, and P. S. Krishnaprasad. Approximate inversion of the Preisach hysteresis operator with application to control of smart actuators. *IEEE Trans. Automatic Control*, 50(6):798–810, 2005.

U. Kunze. Invited review nanoscale devices fabricated by dynamic ploughing with an atomic force microscope. *Superlattices and Microstructures*, 31(1):3–17, 2002.

K. K. Leang and S. Devasia. Design of hysteresis-compensating iterative learning control for piezo positioners: application to atomic force microscopes. *Mechatronics*, 6(3-4):141 – 158, 2006.

K. K. Leang and S. Devasia. Feedback-linearized inverse feedforward for creep, hysteresis, and vibration compensation in AFM piezoactuators. *IEEE Trans. Contr. Syst. Tech.*, 15(5):927 – 935, 2007.

I. D. Mayergoyz. *Mathematical models of hysteresis*. Springer-Verlag, New York, 1991.

K. L. Moore, M. Dahleh, and S. P. Bhattacharyya. Iterative learning control: a survey and new results. *J. Robotic Systems*, 9(5):563–594, 1992.

G. Ortner, M. Bayer, A. Larionov, V.B̃. Timofeev, A. Forchel, Y.B̃. Lyanda-Geller, T.L̃. Reinecke, P. Hawrylak, S. Fafard, and Z. Wasilewski4. Fine structure of excitons in InAs/GaAs coupled quantum dots: A sensitive test of electronic coupling. *Physical Review Letters*, 90:086404, 2003.

R. D. Piner, J. Zhu, F. Xu, S. Hong, and C. A. Mirkin. Dip-pen nanolithography. *Science*, 283:661 – 663, 1999.

S. Salapaka, A. Sebastin, J. P. Cleveland, and M. V. Salapaka. High bandwidth nano-positioner: a robust control approach. *Rev. Sci. Instr.*, 73(9):3232–3241, 2002.

R. C. Smith, C. Bouron, and R. Zrostlik. Partial and full inverse compensation for hysteresis in smart material systems. In *American Control Conference*, volume 4, pages 2750 – 2754, Chicago, Illinois, 2000.

E. S. Snow, P. M. Campbell, and F. K. Perkins. Nanofabrication with proximal probes. *Proc. of the IEEE*, 85 (4):601–611, 1997.

L. L. Sohn and R. L. Willett. Fabrication of nanostructures using atomic-force-microscope-based lithography. *Appl. Phys. Lett.*, 67(11):1552 – 1554, 1995.

G. Song, J. Q. Zhao, and X. Q. Zhou. Tracking control of a piezoceramic actuator with hysteresis compensation using inverse Preisach model. *IEEE/ASME Transactions on Mechatronics*, 10(2):198 – 209, 2005.

C. Taylor, E. Stach, A. Malshe, and G. Salamo. Nanoscale dislocation patterning by ultralow load indentation. *Applied Physics Letters*, 87:073108, 2005.

G. Tchoupo and K. K. Leang. Hysteresis compensation for high-precision positioning of a shape memory alloy actuator using integrated iterative-feedforward and feedback inputs. In *American Control Conference*, pages 4246 – 4253, New York City, 2007.

A. Visintin. *Models of hysteresis*. Longman Scientific and Technical, New York, 1993.

M. Wendel, S. Kuhn, H. Lorenz, J. P. Kotthaus, and M. Holland. Nanolithography with an atomic force microscope for integrated fabrication of quantum electronic devices. *Appl. Phys. Lett.*, 65(14):1775 – 1777, 1994.

R. Wiesendanger. *Scanning probe microscopy and spectroscopy*. Cambridge University Press, Cambridge, 1994.

Y. Wu and Q. Zou. Iterative control approach to compensate for both the hysteresis and the dynamics effects of piezo actuators. *IEEE Control Systems Technology*, 15 (5):936 – 944, 2007.

Y. Yan, T. Sun, Y. Liang, and S. Dong. Investigation on AFM-based micro/nano-CNC machining system. *International Journal of Machine Tools and Manufacture*, 47: 1651 – 1659, 2007.